


Probe-corrected near-field to far-field transformation using multiple spherical wave expansions

Fernando Rodríguez Varela , Belén Galocha Iragüen and
Manuel Sierra Castañer

Universidad Politécnica de Madrid, Av. Complutense no. 30, Madrid, Spain

Research Paper

Cite this article: Rodríguez Varela F, Galocha Iragüen B, Sierra Castañer M (2020). Probe-corrected near-field to far-field transformation using multiple spherical wave expansions. *International Journal of Microwave and Wireless Technologies* **12**, 447–454. <https://doi.org/10.1017/S1759078720000136>

Received: 20 September 2019

Revised: 27 January 2020

Accepted: 30 January 2020

First published online: 27 February 2020

Key words:

Antenna measurements; arbitrary surfaces; near-field to far-field transformation; spherical wave expansion (SWE)

Author for correspondence:

Fernando Rodríguez Varela,
E-mail: f.rodriguez@upm.es

Abstract

Near-field to far-field transformations constitute a powerful antenna characterization technique for near-field measurement scenarios. In this paper, a near-field to far-field transformation technique based on multiple spherical wave expansions (SWEs) is presented. Thanks to its iterative matrix inversion nature, the approach performs the transformation of fields measured on arbitrary surfaces. Also, irregular sampling schemes can be incorporated. The proposed algorithm is based on modeling the antenna fields with not one, but several SWEs distributed over its geometry. Due to the high number of SWEs, their truncation number can be arbitrarily reduced. Working with expansions of low order allows us to incorporate the probe correction in the transformation in a very simple way, accepting any type of probe and orientation. Only the probe far-field pattern is used, thus working with its full SWE is avoided. The algorithm is validated using simulated field data as well as measurements of real antennas.

Introduction

Antenna near-field measurements constitute a versatile tool for determining antennas radiation pattern. This type of measurement requires the use of post-processing techniques to transform the antenna under test (AUT) measured near-fields into the radiated far-field. Traditionally, near-field measurements have been performed using canonical acquisition surfaces to simplify the post-processing steps: spheres, cylinders, and planes. Among the three, the spherical measurement system has been regarded as one of the most accurate and powerful techniques [1]. With the growing interest in high frequencies and robotic positioning equipment [2], achieving correct probe location and orientation becomes challenging. In addition, there exists an increasing trend in measurement set-ups where the antenna near-field is measured in a surface of arbitrary shape and sampling enclosing the AUT, as in the case of over-the-air measurements [3]. Near-field to far-field transformation algorithms suitable for these scenarios must be implemented, as the classical post-processing techniques cannot be applied in these cases.

Several approaches have been proposed for the transformation of fields measured over canonical surfaces with irregular sampling. The use of non-equispaced fast Fourier transform has proven to be an efficient way of processing spherical near-field measurements with irregular grids due to positioning errors [4]. Optimal sampling interpolation techniques have also been proposed for planar [5], cylindrical [6], and spherical [7] acquisition surfaces. In this case, the fields are measured over a non-redundant grid of points and then interpolated to a regular grid that can be processed by classical near-field to far-field transformation algorithms.

More flexible transformation techniques that can deal with both irregular sampling and arbitrary surfaces have also been reported. Most of them consist of a two-step procedure: first, an equivalent representation of the AUT is found by solving an inverse problem with the knowledge of the near field. This involves solving a system of equations usually formulated in matrix form. Then, the far-field of the equivalent representation is computed to obtain the AUT radiation pattern. Depending on the type of equivalent representation used (magnetic/electric currents [8], spherical waves [9], and complex source beams [10]) different approaches can be followed to formulate the problem and reduce the number of operations. Solving the inverse problem can turn into a computationally intensive task, particularly for electrically large antennas. As the electrical size of the problem increases, the number of measurement points grows quadratically, and so does the size of the problem matrix with respect to the number of points. This results in an overall scalability of $O(n^4)$, which limits the applicability of some of these techniques to small and medium problems. Mathematical and computational

improvements are still needed for the transformation of fields measured over arbitrary surfaces with irregular sampling.

In this paper, a new technique to address this type of near-field to far-field transformation problem is proposed. It can process near field measured over arbitrary surfaces and grids with full probe correction. The main novelty is the use of a multiple spherical wave expansion (SWE) representation to model, the AUT. This is done by defining a set of unknown SWEs centered around the antenna shape, as opposed to the conventional approach based on a single SWE centered at the coordinate system origin. The advantage of using several expansions is that the probe-correction can be applied using directly the probe’s far-field pattern without having to deal with its own SWE and complex translation and rotation coefficients. In addition, the approach is suitable for a multi-level extension, which can reduce the algorithm computational complexity drastically.

The structure of this paper is as follows. In Section “Near-field to far-field transformation theory,” the basic theory of the multiple SWE field transformation algorithm is presented. In Section “Numerical transformation results,” the approach is validated based on simulations of antenna fields, leaving the verification with real measured data for Section “Transformation of near-field measured data.” “Conclusion” section concludes this paper.

Near-field to far-field transformation theory

This section deals with the mathematical development for the near-field to far-field transformation technique. First, the use of several SWEs to model the antenna is shown. A transmission formula is derived to compute the interaction between AUT and probe. Finally, a multilevel scheme is proposed to reduce the computational complexity of the inverse problem.

AUT-probe interactions using multiple SWE

The field \vec{E} radiated by a given antenna admits a SWE [11] that can be centered at an arbitrary point \vec{r}_i :

$$\vec{E}(\vec{r}) = \sum_{s=1}^2 \sum_{n=1}^N \sum_{m=-n}^n Q_{smn} \vec{F}_{smn}^{(3)}(\vec{r} - \vec{r}_i) \tag{1}$$

where $\vec{F}_{smn}^{(3)}(\vec{r})$ are the spherical vector wave functions; Q_{smn} the antenna spherical coefficients, and N the truncation number of the expansion. This truncation number is related to the degrees of freedom needed to model the antenna field variations and it is proportional to its size. The bigger the antenna is, the more variations will experiment the radiated field and thus, more spherical harmonics are needed to model it. In particular, there exists the following rule of thumb:

$$N_l = ka_l + 10 \tag{2}$$

where a_l is the radius of the smallest sphere circumscribing sub-domain l (minimum sphere), k the free space wavenumber, and the brackets indicate the largest integer smaller than or equal to the number inside them.

Conventionally, \vec{r}_i is set to 0 and the coordinate system is centered at the antenna system to minimize N and so, the number of terms in the summation. In this case, a different approach will be taken, as the field $\vec{E}(\vec{r})$ can be modeled also using not one, but

several SWEs centered at different points \vec{r}_i :

$$\vec{E}(\vec{r}) = \sum_{i=1}^I \sum_{s=1}^2 \sum_{n=1}^{N_i} \sum_{m=-n}^n Q_{smn}^i \vec{F}_{smn}^{(3)}(\vec{r} - \vec{r}_i) \tag{3}$$

The combination of several SWEs creates new field variations so each individual SWE needs now a lower truncation number N_i than in the previous case. The lower the values of N_i used, the smaller the number of harmonics will have each expansion, so more expansions are needed to model adequately the field variations.

In a real measurement scenario, it is not possible to measure directly the AUT field $\vec{E}(\vec{r})$ since the antenna used as probe has some influence. The probe has its own SWE that can be introduced in the above formulation to consider its effect. The probe SWE coefficients must be rotated and translated depending on its location and orientation leading to complex calculations. In addition, if the probe exhibits non-ideal orientations, more rotations are needed [12]. However, if the truncation number of the expansions N_i is set to a low value compared to the probe distance, the signal measured by the probe can be approximated by:

$$w(\vec{r}) \approx \sum_{i=1}^I \vec{P}(\vec{r}_i - \vec{r}) \sum_{s=1}^2 \sum_{n=1}^{N_i} \sum_{m=-n}^n Q_{smn}^i \vec{F}_{smn}^{(3)}(\vec{r} - \vec{r}_i) \tag{4}$$

Being $\vec{P}(\vec{r})$ the probe radiation pattern: Note that $\vec{r}_i - \vec{r}$ represents the angular direction of the i th SWE seen from the probe placed at \vec{r} . Therefore, it can be considered that the measured signal $w(\vec{r})$ is a superposition of the contributions of each SWE weighted by the probe radiation pattern in the angular direction where the SWE is seen from the probe. It is important to consider that with this approach we are reducing the AUT near-field field effect but not for the probe. This can be a limiting factor in scenarios where the probe is very close to the AUT, although in most cases the probe size is small compared to the measurement distance.

Equation (4) can be expressed as a matrix-vector product:

$$W = CQ \tag{5}$$

being W a vector that contains the probe measurements in all the acquisition points, Q the vector that contains the coefficients of all SWEs, and C the coupling matrix that performs the summation and multiplications. Our problem is to determine Q from the field measurements W , so we can evaluate the equivalent representation Q at the far-field using the asymptotic form of (3) when $\vec{r} \rightarrow \infty$.

Equation (5) is solved in the least squares sense by computing:

$$Q = (C^H C)^{-1} C^H W \tag{6}$$

Due to the high number of unknowns involved, an iterative matrix inversion method such as conjugate gradient (CG) [13] is preferred over a direct inversion. To obtain a valid solution, well distributed and sampled measurements W are needed for two orthogonal polarizations. There are no further restrictions, so the method is suitable for arbitrary measurement grids with irregular sampling.

The CG is an iterative algorithm which starts with an initial guess of the solution, Q_0 , and gradually approaches the correct

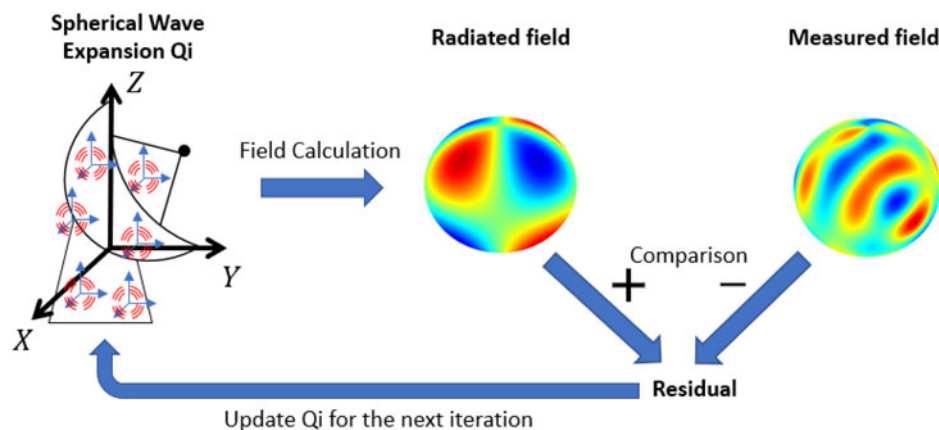


Fig. 1. Representation of one step in the CG algorithm to obtain the coefficients for the equivalent SWEs.

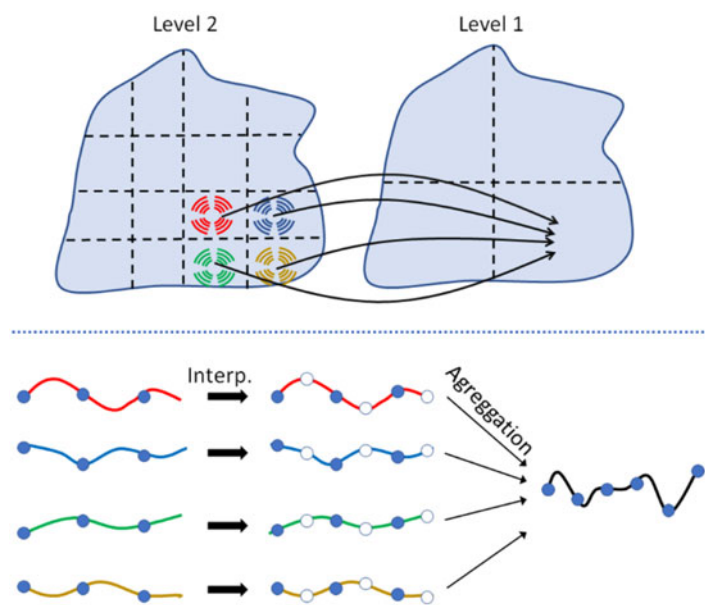


Fig. 2. Schematic representation of the multilevel spherical wave aggregation process.

solution Q , obtaining a residual $W - CQ_i$ on each iteration i . From this residual, the solution vector Q_i is updated for the next iteration. When the residual is low enough the algorithm is stopped. Figure 1 shows a schematic representation of one step in the CG for this particular problem. We start with a guess Q_i for the coefficients of all SWEs and calculate the field radiated by these guess coefficients, CQ_i . This radiated field is compared with the measured field W , obtaining a residual that is used to update Q_i for the next iteration. From these steps, the radiated field calculation is the most computationally intensive, therefore, in the next section an efficient implementation for this step will be proposed.

Multilevel spherical wave aggregation

This section deals with an efficient implementation of the iterative inversion algorithm for solving (6). When working with explicit matrices, the overall cost of the inverse process is around $O(d^4)$, d being the electrical size of the AUT. However, the matrix multiplications inside the iterative algorithm can be replaced by fast operators that compute matrix vector products on the fly. In particular, we focus on the product $W = CQ$. This calculation is

performed repeatedly in the CG algorithm until a good level of convergence is reached. As shown in the previous section, matrix-vector product CQ can be understood as the radiation of a set of multiple SWE measured by a probe antenna. The multilevel spherical wave aggregation performs this computation without the need of matrix operators, using interpolation and a multilevel aggregation scheme.

The field radiated by an AUT of finite size can be sampled on a non-redundant grid of points given by a sampling rate. This sampling rate depends on the electrical size of the AUT. A common criterion [11] is to use angular increments $\Delta\theta = \Delta\varphi = \pi/N$, where N is defined in (2) as a function of the minimum sphere. This means that the smaller the AUT, the less samples are required to store the radiated field. Using this concept, we will devise a scheme for an efficient calculation of the fields radiated by the AUT, i.e. $W = CQ$. First, we calculate the fields radiated by each SWE on a non-redundant grid of points. Then, from this grid, the fields are interpolated to the measurement grid. In order to obtain a good computational complexity, this interpolation must be performed in a multilevel scheme: the SWEs are grouped progressively, and, as the size of the group increases, the fields are interpolated and aggregated.

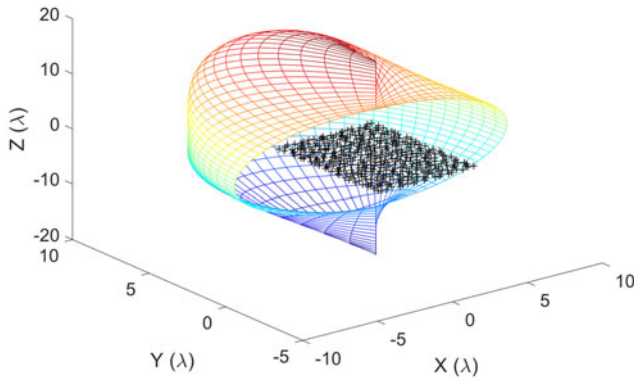


Fig. 3. Dipole distribution and measurement surface for the near-field.

The interpolation–aggregation procedure is explained using a simple example. Assume an AUT that is modeled using $4 \times 4 = 16$ local SWEs and its field has been measured according to the Nyquist criterion in a spherical grid of $N_\theta \times N_\varphi = 64 \times 128$ points. In a given iteration of the CG, we must calculate the field radiated by the SWE of that iteration and compare it with the measured field. Because each SWE is roughly four times smaller in each dimension than the total AUT, the radiated fields can be calculated in four grids of 16×32 points, one grid per SWE. Now, we move to the next level and group the adjacent SWE in 2×2 groups. Each group contains four SWEs, so the field of each group is the linear combination of the SWE fields. Because the groups have double their size, the Nyquist rate is also doubled. Therefore, the fields are interpolated to a 32×64 grid before being aggregated. At the end of this step we have 2×2 grids of 32×64 points, one grid per SWE. The final step is the aggregation of the four groups into a single one following the same procedure. First, the fields sampling rate is doubled and then the fields are combined, obtaining a grid of 64×128 , which is virtually the field of the complete AUT. Note that we can perform this interpolation with arbitrarily low error because the fields are sampled at the Nyquist rate in all steps of the algorithm. It can be shown that this process is more efficient than directly computing the fields of each SWE in a 64×128 grid and then combining the 16 grids.

Figure 2 depicts a schematic representation of the first step in the multilevel aggregation process for the AUT of the previous example. At this point we are in the level 2 of the algorithm. To move on to level 1, the SWEs are aggregated in groups of 4, so the fields radiated by each of them are combined. Before adding the fields, they need to be interpolated because the electrical size of the group has increased. This interpolation–aggregation procedure is repeated until all groups have been combined and the field of the complete AUT is obtained. It can be shown that this multi-level scheme reduces the computational complexity of the problem from $O((kr_0)^4)$ when conventional matrix–vector products are used, to $O((kr_0)^2 \log(kr_0))$.

Numerical transformation results

The capabilities of the proposed transformation algorithm are validated using a simulation example with analytical data. Considered is a distribution of 600 Hertzian dipoles randomly placed at plane $z = 0$ and fed by voltages ranging between 0 and 1 V. The distribution has an approximate size of $3\lambda \times 3\lambda$. The electric field radiated by the distribution is measured over a non-

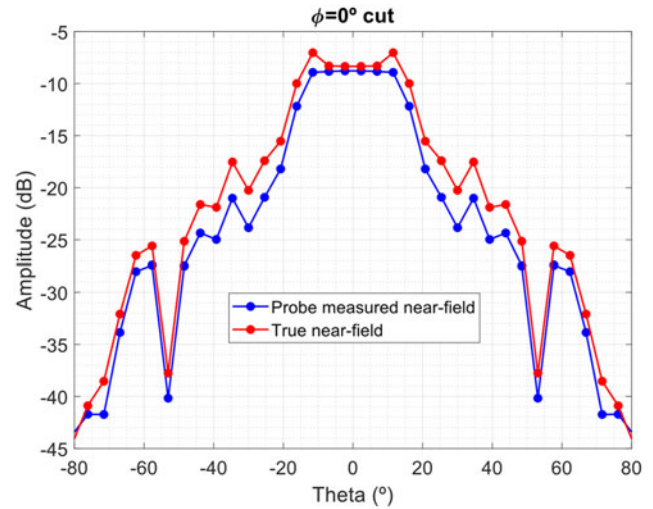


Fig. 4. Comparison of the radiated near-field and the measured field by a directive probe. The latter is used as an input for the transformation algorithm.

canonical surface given by the following parametric expression in spherical coordinates:

$$r(\theta, \varphi) = 8(1 + (\cos \theta \sin \varphi)^2)\lambda \quad (7)$$

with a sampling of 40 points in θ and 80 in φ . Figure 3 depicts the dipole distribution (in black) and the acquisition surface cut in half for better visualization.

The probe antenna used is modeled with a radiation pattern following a $\cos^q \theta$ pattern with $q = 8$. The probe has been selected to be directive for better demonstration of the algorithm probe correction capabilities. The effect of the probe influence can be appreciated as in Fig. 4 where a $\varphi = 0^\circ$ field cut has been depicted, along with the signal measured by the probe. The effect is significant as the measurement surface is very close to the AUT.

To perform the near-field to far-field transformation, the antenna is modeled as a set of SWEs centered at $z = 0$ covering its surface. As mentioned in the previous section, the number of expansions needed depends on the truncation number N_i . Two cases of truncation number have been investigated for this example $N_i = 2$ and $N_i = 6$ for all expansions. In Fig. 5 the AUT is depicted for the two cases, where the dipoles are represented with black crosses. Over the surface of the AUT, the local SWEs are placed. The centers of each SWE are signaled in red and it can be seen that they are uniformly distributed over the aperture. Because the AUT is mainly planar, the SWEs are only distributed over the AUT aperture plane. It is observed that the case of $N_i = 2$ requires smaller spacing between SWEs since the modal content of the expansions is lower than in the case of $N_i = 6$. With this SWE distribution, matrix C is built and vector W is populated with the values measured by the probe.

The near-field to far-field transformation is performed for the two cases using the CG algorithm to obtain the coefficients of each SWE. The transformed far-field is compared with the true far-field of the array distribution to obtain the transformation error. This true far-field is computed analytically using the asymptotic evaluation of the dipole fields. In Fig. 6 the difference between the transformed far-field and the true far-field for the two cases has been depicted along with the true far-field. In addition, the error of a non-probe-corrected transformation has been

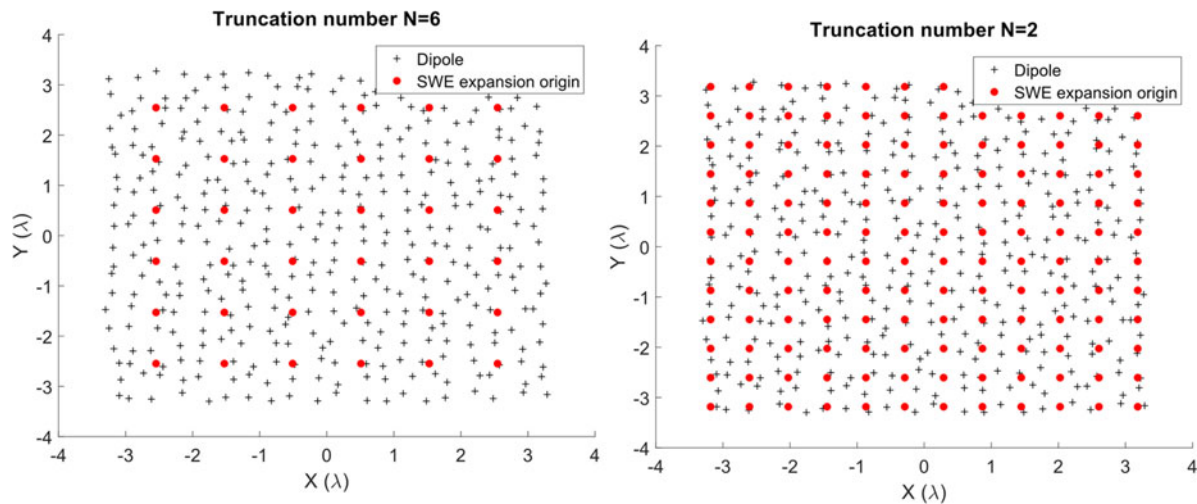


Fig. 5. Different configurations for the same dipole array antenna.

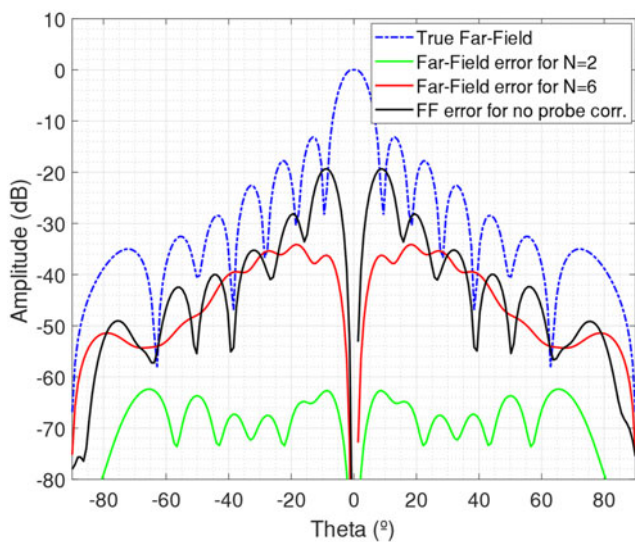


Fig. 6. Transformed far-field errors for the two configurations of Fig. 5 and for the case of no probe correction.

added. It can be seen that neglecting the probe effect yields an error with a level of roughly -10 dB with respect to the reference field. Using multiple SWEs allows us to include the probe effect reducing this error significantly.

However, there exists some residual error due to the approximation made in (3). This approximation is more ambitious for the case of $N_i=6$ and the error exhibited is still relevant. For less directive probes and/or larger measurement distances, higher values of N_i could be used maintaining negligible transformation error levels. If the probe distance is large enough, a single SWE could give enough accuracy and the proposed algorithm would be identical to the approach proposed in [5].

Transformation of near-field measured data

Finally, the proposed algorithm is verified using actual near-field data to check its stability against noise and practical inaccuracies. As a first test, a reflector antenna of diameter 60 cm is measured

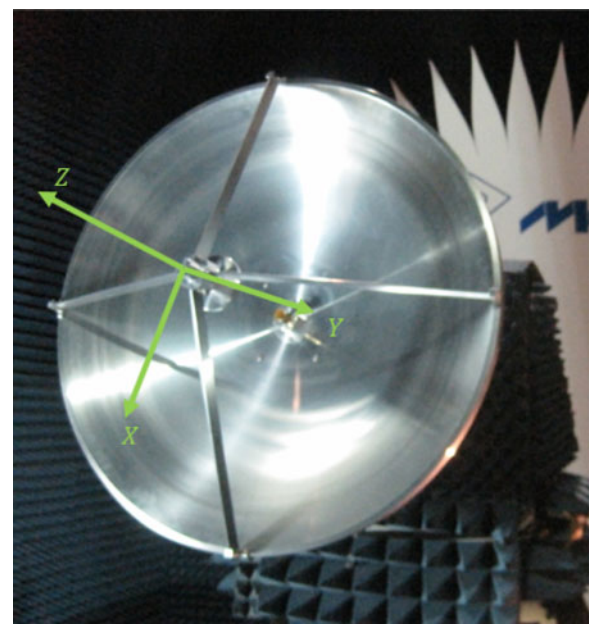


Fig. 7. Antenna used for the algorithm verification and coordinate system definition.

operating at 8 GHz. Since hardware was not available to generate a measurement surface different than a sphere, plane, or cylinder or with irregular sampling, the selected shape has been a half sphere. This acquisition is generated performing a standard spherical near-field measurement truncating the rest of the sphere. Naturally, the truncated part corresponds to the backside of the antenna, so that most of the radiated field is kept. This corresponds to the region $\theta \leq 90^\circ$ (see Fig. 7 for the axes definition). The sampling rate is given by the standard spherical criterion $\Delta\theta = \Delta\varphi = \pi/N$.

Measurements for two orthogonal polarizations are performed at a distance of 5 m. At this distance, the probe effect is small, but the algorithm is taken to the limit using local SWEs of minimum order $N_i=1$. The approximate spacing between SWEs is set to around 0.35λ . From the measurements and problem geometry, vector W and matrix C are populated respectively, and the CG algorithm is started.

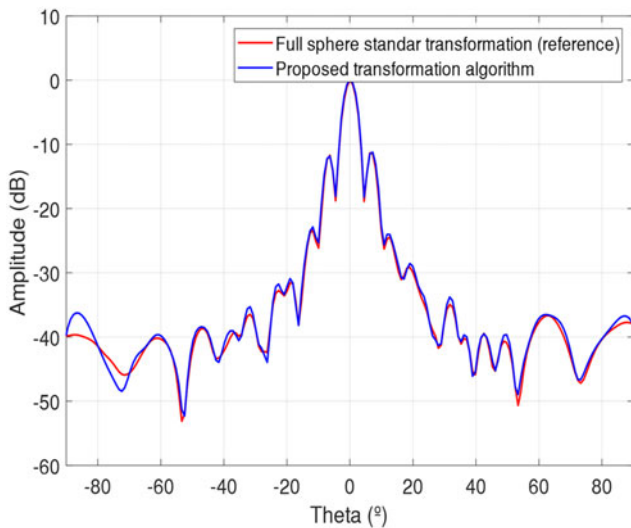


Fig. 8. Comparison of the transformed far-field using the proposed algorithm with a truncated sphere and a classical transformation using the complete sphere.

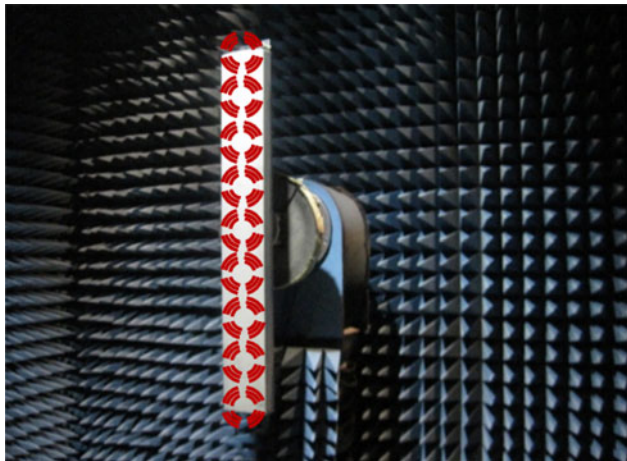
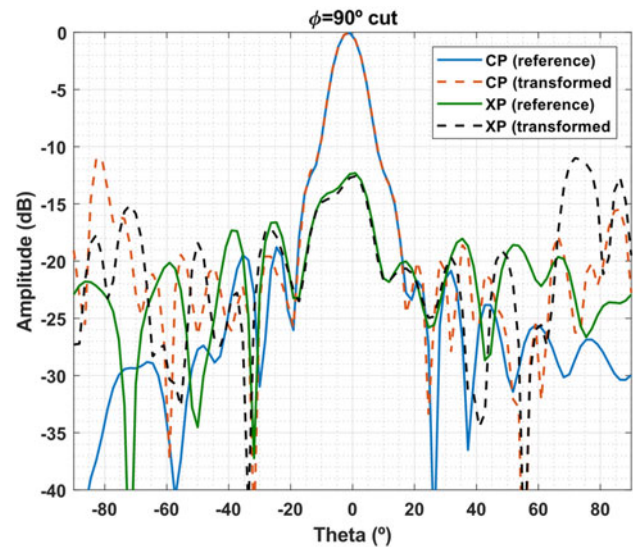


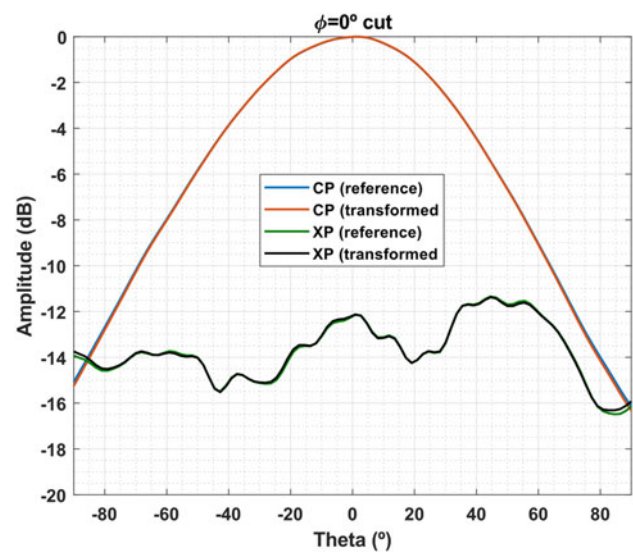
Fig. 9. Representation of how the local SWEs are placed to model the base station antenna.

After the evaluation of the CG, the coefficients of all SWEs are obtained and then can be evaluated at far-field to obtain the antenna radiation pattern. A $\varphi = 0^\circ$ cut of this field is shown in Fig. 8 along with the transformed field using a classical spherical near-field to far-field transformation with the information of the complete measurement sphere. The agreement between the two fields is good with values near to $\theta = 90^\circ$ though there exist small differences due to the truncation of the scan sphere. For θ values larger than 90° , the proposed algorithm was unable to extrapolate the field, as this corresponds to the truncated solid angle region, so the results have not been depicted.

The second test is a base station antenna working at 1.9 GHz measured in a cylindrical near-field scanner. The dimensions of the cylinder are 0.6 m in radius and 3.5 m in height. The field is sampled with 23 z samples by 36 in φ , which corresponds to the standard sampling rate of cylindrical near-field measurements by the given AUT and cylinder sizes [14]. The AUT dimensions are roughly $180 \times 20 \times 20$ cm. Its volume is modeled by nine local SWEs of $N_i = 5$ arranged in a line as depicted in Fig. 9.



(a)



(b)

Fig. 10. Comparison of the transformed far-field main cuts using the proposed algorithm with a cylinder and a classical transformation a sphere.

The proposed algorithm is applied to process the cylindrical field and the obtained far-field is depicted in Fig. 10 for the $\varphi = 0^\circ$ and $\varphi = 90^\circ$ cuts. In addition, a standard spherical near-field measurement of the same antenna is performed to obtain the far-field of the antenna with maximum accuracy and use it as a reference. This reference radiation pattern is also depicted in Fig. 10. As it can be seen, the horizontal plane shows perfect agreement because all the radiation is measured on this cut. On the vertical plane, the radiation pattern shows significant differences for elevation angles higher than 30° due to the truncation of the cylinder.

As a final test, to verify the functionality of the proposed algorithm with no field truncation, a 1 GHz 2×2 patch array antenna is measured in a spherical near-field system. The distance between probe and AUT is 5 m. The field is measured with an angular sampling of $\Delta\theta = \Delta\varphi = 6^\circ$ in two orthogonal polarizations. A $2\lambda \times 2\lambda \times 2\lambda$ cube enclosing the AUT is used as equivalent

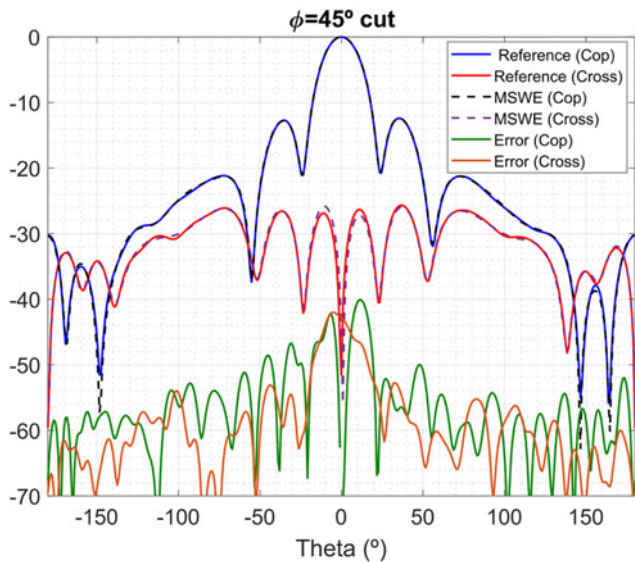


Fig. 11. Patch array co- and cross-polar transformed far-field patterns.

surface. This cube is modeled by 16 local SWEs of $N_i = 5$ distributed on the cube faces and the far-field is transformed. For reference, the far-field transformed with the commercial software SNIFT [15] is used. Figure 11 depicts the co-polar and cross-polar patterns of a $\phi = 45^\circ$ cut. The transformation errors are quite small obtaining an excellent agreement.

Conclusion

A near-field to far-field transformation algorithm for arbitrary acquisition surfaces is presented. The algorithm is based on modeling the AUT as a set of unknown multiple SWEs distributed over the antenna surface. The coefficients of all SWEs are found by solving an inverse problem and when found, the field can be evaluated at the asymptotically to obtain the radiation pattern straightforwardly. It has been shown that with careful choosing of the SWE location and truncation index, the probe effect can be accounted with almost no additional effort without needing to deal with is spherical coefficients and complex rotations.

In addition, using multiple SWEs to model the antenna radiation makes the problem suitable for a multi-level scheme. During the inversion problem, the interaction of near SWEs with the probe can be aggregated in groups following a multilevel structure to speed up the calculations. This procedure helps to reduce the computational complexity of the calculations drastically.

The algorithm has been verified using simulated and measured data from real antennas, showing low transformation errors and promising capabilities.

Acknowledgement. The authors would like to acknowledge Universidad Politécnica de Madrid, the Spanish Government, Ministry of Economy, National Program of Research, Development and Innovation for the support of this publication in the projects ENABLING-5G “Enabling innovative radio technologies for 5G networks” (project number TEC2014-55735-C3-1-R) and FUTURE-RADIO “Radio systems and technologies for high capacity terrestrial and satellite communications in a hyper-connected world” (project number TEC2017-85529-C3-1-R) and Madrid Region Government for the project S2013/ICE-3000 (SPADERADAR-CM).

References

1. Breinbjerg O (2016) Spherical near-field antenna measurements – the most accurate antenna measurement technique, *IEEE International Symposium on Antennas and Propagation*, Puerto Rico, pp. 1019–1020, June 2016.
2. Hatzis J, Pelland P and Hindman G (2016) Implementation of a combination planar and spherical near-field antenna measurement system using an industrial 6-axis robot, *AMTA 2016 Proceedings*, Austin, TX, USA, 2016, pp. 1–6.
3. Fernandez MG, Lopez YA and Andres FL (2018) On the use of unmanned aerial vehicles for antenna and coverage diagnostics in mobile networks. *IEEE Communications Magazine* 56, 72–78.
4. Wittmann RC, Alpert BK and Francis MH (2004) Near-field, spherical scanning antenna measurements with nonideal probe locations. *IEEE Transactions on Antennas and Propagation* 52, 2184–2187.
5. D’Agostino F, Ferrara F, Gennarelli C, Guerriero R and Migliozi M (2017) Fast and accurate far-field prediction by using a reduced number of bipolar measurements. *IEEE Antennas and Wireless Propagation Letters* 16, 2939–2942.
6. D’Agostino F, Ferrara F, Gennarelli C, Gennarelli G, Guerriero R and Migliozi M (2012) On the direct non-redundant near-field-to-far-field transformation in a cylindrical scanning geometry. *IEEE Antennas and Propagation Magazine* 54, 130–138.
7. D’Agostino F, Ferrara F, Gennarelli C, Guerriero R and Migliozi M (2013) Non-redundant spherical NF – FF transformations using ellipsoidal antenna modeling: experimental assessments [measurements corner]. *IEEE Antennas and Propagation Magazine* 55, 166–175.
8. Sarkar TK and Taaghola A (1999) Near-field to near/far-field transformation for arbitrary near-field geometry utilizing an equivalent electric current and MoM. *IEEE Transactions on Antennas and Propagation* 47, 566–573.
9. Farouq M, Serhir M and Picard D (2016) Antenna far-field assessment from near-field measured over arbitrary surfaces. *IEEE Transactions on Antennas and Propagation* 64, 5122–5130.
10. Chou H, Pathak PH, Tuan S and Burkholder RJ (2017) A novel far-field transformation via complex source beams for antenna near-field measurements on arbitrary surfaces. *IEEE Transactions on Antennas and Propagation* 65, 7266–7279.
11. Hansen JE (1988) *Spherical Near-Field Antenna Measurements*. London, UK: Peter Peregrinus.
12. Cornelius R and Heberling D (2017) Correction of non-ideal probe orientations for spherical near-field antenna measurements, *AMTA 2017 Proceedings*, Atlanta, GA, pp. 1–5.
13. Y. Saad (2003) *Iterative Methods for Sparse Linear Systems*, 2nd Edn. Philadelphia, PA, USA: Society for Industrial and Applied Mathematics.
14. Leach WM and Paris DT (1973) Probe-compensated near-field measurements on a cylinder. *IEEE Transactions on Antennas and Propagation* AP-21, 435–445.
15. SNIFT Software, TICRA, Copenhagen, Denmark. Available at <http://www.ticra.com>.



Fernando Rodríguez Varela was born in 1994 in Ourense, Spain. He received his M.Sc. degree in Telecommunication Engineering from the Technical University of Madrid, in 2018, where he is currently pursuing his Ph.D. degree on near-field to far-field transformation techniques. His current research interests include antenna design and antenna measurement and post-processing techniques.



Belén Galocha Iragüen was born in 1964 in Bretoña (Lugo), Spain. She received her Electrical Engineering and Ph.D. degrees, both from the Technical University of Madrid (UPM), Madrid, Spain, in 1988 and 1992, respectively. Since 1992, she has been with the Radiation Group of Signals, Systems and Radio-Communications Department at UPM as an Associate Professor. Her current research

interests include horn antennas, aperture antennas, and microwave passive devices.



Manuel Sierra Castañer was born in 1970 in Zaragoza (Spain). He obtained a degree in Telecommunication Engineering in 1994 and his Ph.D. in 2000, both from the Technical University of Madrid (UPM) in Spain. Since 1998 he has been working at the Technical University of Madrid as research assistant, assistant, Associate and Full Professor. His current research interests are in planar antennas

and antenna measurement systems. Dr. Sierra Castañer received the IEEE APS 2007 Schelkunoff Prize paper Award for the paper “Dual-Polarization Dual-Coverage Reflectarray for Space Applications” in 2007. He is member of the Board of Director of European Association of Antennas and Propagation since 2016, where he is currently vice-chair, and AMTA Europe Liaison since 2015.